Electronic Supplementary Information

A Distorted [Mn$_2$(COO)$_4$N$_2$] Cluster Based Metal−Organic Framework with (3,3,6) Topology and Selective Adsorption of CO$_2$

Jingjing Jiang,[1] Qian Wang,[2] Mingxing Zhang[1] and Junfeng Bai*[,2,1]

[1]*State Key Laboratory of Coordination Chemistry, School of Chemistry and Chemical Engineering, Nanjing University, Nanjing 210023, China*

[2]*School of Chemistry and Chemical Engineering, Shaanxi Normal University, Xi'an 710119, China*

E-mail: bjunfeng@nju.edu.cn. Tel: +86-25-89683384.

Table of contents

I. Synthesis of ligand and MOF

General procedures. All reagents were obtained from commercial vendors and, unless otherwise noted, were used without further purification. Elemental analysis (C, H, N) were carried out with a Elementar Vario MICRO Thermo. The IR spectra were obtained in the 4000~400 cm^{-1} on a VECTOR TM 22 spectrometer using KBr pellets. ^{1}H NMR spectra were recorded on a Bruker DRX-300 spectrometer with tetramethylsilane as an internal reference. Thermal gravimetric analyses (TGA) were performed under N$_2$ atmosphere (100 ml/min) with a heating rate of 5 °C/min using a 2960 SDT thermogravimetric analyzer. Powder X-ray diffraction (PXRD) data were collected on a Bruker D8 ADVANCEX-ray diffractometer with Cu Kα radiation.
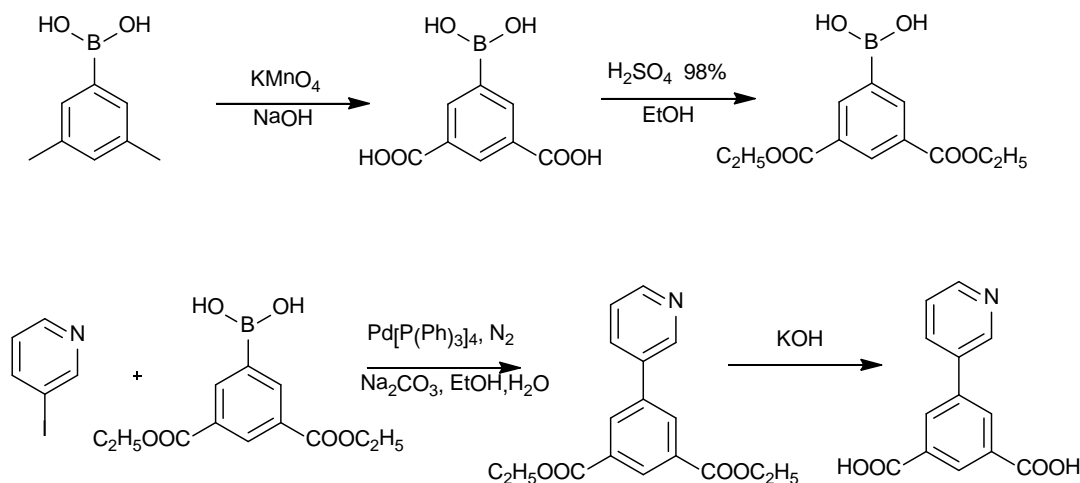
Scheme 1.The synthetic route of **H₂L**

Synthesis of benzene-3,5-dicarboxyelester-boronic acid. This compound was prepared according to reported procedure[1]: 3,5-dimethylphenylboronic acid (10 g, 67 mmol) and NaOH (5 g, 125 mmol) were dissolves in tert-butanol/water (v/v = 1:1; 250 mL). The reaction mixture was heated to 50°C with stirring, and small portions (1 g) of KMnO$_4$ were added to the solution. After the color from red to brown, added the rest of KMnO$_4$ (65 g), raised the temperature to 70°C, and added additional of KMnO$_4$ (6 g). There action continued until the brown color persisted for 3 hours. The excess KMnO$_4$ was reduced by addition of Na$_2$S$_2$O$_3$ (1 g) and then filtered when hot. The filtrate concentrated to ~ 150 mL by evaporation and acidified to pH = 1 using concentrated HCl. The white precipitate was separated by filtration, washed with water, and freeze-dried. The dried white solid was mixed with 98% H$_2$SO$_4$ (6 mL) in anhydrous EtOH (150 mL), and the solution refluxed for 12 hours.

Synthesis of 5-(pyridin-3-yl) isophthalic acid (H₂L). To a solution of 3-Iodopyridine (2.05 g, 10 mmol) in 125 mL of toluene was added the mixture of 3,5-bis(methoxy-carbonyl)phenylboronic acid

(3.45 g, 13 mmol) in 30 mL of ethanol, followed by the addition of a solution of Na_2CO_3 (3.7g, 35.4 mmol) in 10 mL of water. This solution was degassed using N_2 for 10 min, and then $Pd(PPh_3)_4$ (0.5 g, 0.43 mmol) was added. The resulting reaction mixture was stirred at 85 °C under N_2 overnight. The solvent was then removed using rotary evaporation, and the residue was dissolved in CH_2Cl_2 and washed with water. The organic layer was next dried over $MgSO_4$, filtered, concentrated, and purified by silica gel flash column chromatography with an eluent of acetone : petroleum ether = 1:13.5 (v/v). The product was hydrolyzed by refluxing in 2 M aqueous KOH followed by acidification with 37% HCl to afford a white solid, **H_2L**. Yield = 2.1g (86.4%). IR (KBr, cm^{-1}): 3086, 1716, 1622, 1600, 1593, 1478, 1451, 1388, 1307, 1286, 1269, 1237, 1144, 1039, 924, 906, 805, 866, 697, 680, 606. ^1H NMR (300 MHz, DMSO-d_6, δ ppm): 13.47 (s, 2H, COOH), 8.97 (s, 1H, PyH), 8.66 (d, J = 1.95Hz, 1H, PyH), 8.51 (s, 1H, ArH), 8.43 (s, 2H, ArH), 8.22 (d, J = 7.98Hz, 1H, PyH), 7.54 ~ 7.59 (m, 1H, PyH).

Synthesis of [$Mn_2(L)_2DMF$]·DMF·$MeOH$ (NJU-Bai33). A solution of $MnCl_2$·$4H_2O$ (20.0 mg, 0.1 mmol) in 0.5 mL of methanol was mixed with the H_2L (10 mg, 0.04mmol) in 1.5 mL of N,N'-dimethylformamide. To this was added 0.01 mL of concentrated HCl with stirring. The mixture was sealed in a Pyrex tube and heated to 120℃ for 48h. The colorless block crystals obtained were filtered and washed with DMF. Yield = 76.6 %. Selected IR (cm^{-1}): 3125, 1679, 1660, 1625, 1562, 1482, 1444, 1400, 1381, 1293, 1245, 1191, 1104, 1042, 916, 874, 816, 774, 720, 678, 655, 636. Elemental analysis (%) calcd. for $C_{33}H_{32}Mn_2N_4O_{11}$: C 51.44, H 4.18, N 7.27; found: C 52.3, H 4.15, N 7.08.

Sample activation. The as-synthesized sample of NJU-Bai33 was soaked in acetone for 3 days with acetone refreshing every 8 hours. Then, the acetone-exchanged sample was activated at 110 °C and under vacuum for 10 hours. *Note*: Upon exposure to air, the pore channels in the desolvated sample of NJU-Bai33 may be occupied by moisture. Elemental analysis (%) calcd. for $C_{26}H_{22}Mn_2N_2O_{12}$ (desolvated NJU-Bai33·$4H_2O$): C 47.01, H 3.34, N 4.22; found: C 47.44, H 3.55, N 4.22. The water molecules in the analytical data were present because water was readsorbed from air during measurement preparations.[2,3]

II.   X-ray single crystal structure determination

Single-crystal X-ray diffraction data were measured on a Bruker Apex II CCD diffractometer at 150 K using graphite monochromated Mo/Kα radiation (λ = 0.71073 Å). Data reduction was made with the Bruker SAINT program. The structures were solved by direct methods and refined with full-matrix least squares technique using the SHELXTL package[4a]. Non-hydrogen atoms were refined with anisotropic displacement parameters during the final cycles. Organic hydrogen atoms were placed in calculated positions with isotropic displacement parameters set to $1.2 \times U_{eq}$ of the attached atom. The unit cell includes a large region of disordered solvent molecules, which could not be modelled as discrete atomic sites. We employed PLATON/SQUEEZE[4b] to calculate the diffraction contribution of the solvent molecules and, thereby, to produce a set of solvent-free diffraction intensities; structures were then refined again using the data generated.

A summary of the crystallographic data are given in Table S1. CCDC1447021 contains the supplementary crystallographic data for NJU-Bai33. The data can be obtained free of charge at www.ccdc.cam.ac.uk/conts/retrieving.html or from the Cambridge Crystallographic Data Centre, 12, Union Road, Cambridge CB2 1EZ, UK.

Table S1. Crystallographic Data of NJU-Bai33

MOFs	NJU-Bai33
Empirical formula	$C_{29} H_{21} Mn_2 N_3 O_9$
Formula weight	665.37
T [K]	150(2)
Wavelength [Å]	0.71073
Crystal system	Monoclinic
Space group	*Cc*
a [Å]	14.107(3)
b [Å]	15.163(3)
c [Å]	17.765(3)
α [deg]	90
β [deg]	111.025(3)
γ [deg]	90
V [Å^3]	3547.0(12)
Z	4
ρ_{calc}[g cm^{-3}]	1.246
μ [mm^{-1}]	0.760
F(000)	1352
Crystal size [mm^3]	$0.35 \times 0.31 \times 0.25$
Theta range [deg]	$2.05 - 28.29$
Limiting indices	$-18 <= h <= 17$
	$-20 <= k <= 18$
	$-23 <= l <= 20$
Reflections collected	12232
Reflections unique	8824
Completeness	99.4 %
Data/restraints/parameters	6040 / 327 / 413
Goodness-of-fit on F^2	1.097
R1, wR2[a] [I>2σ(I)]	0.0874, 0.2161
R1, wR2[a][all data]	0.0906, 0.2161
$\Delta\rho_{max}$ / $\Delta\rho_{min}$[e. Å^{-3}]	-1.32 / 2.0

[a] $R1 = \Sigma||F_o| - |F_c||/|F_o|$; $wR2 = [\Sigma w(\Sigma F_o^2 - F_c^2)^2/\Sigma w(F_o^2)^2]^{1/2}$.
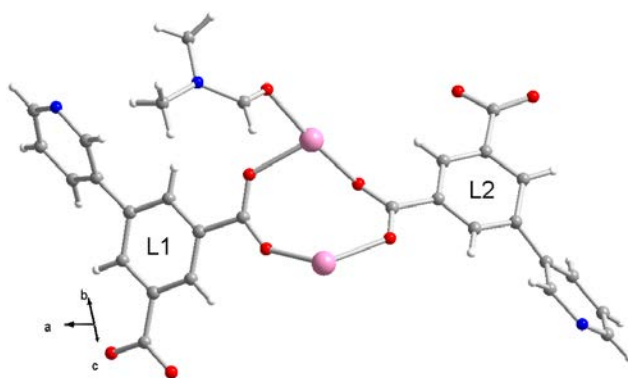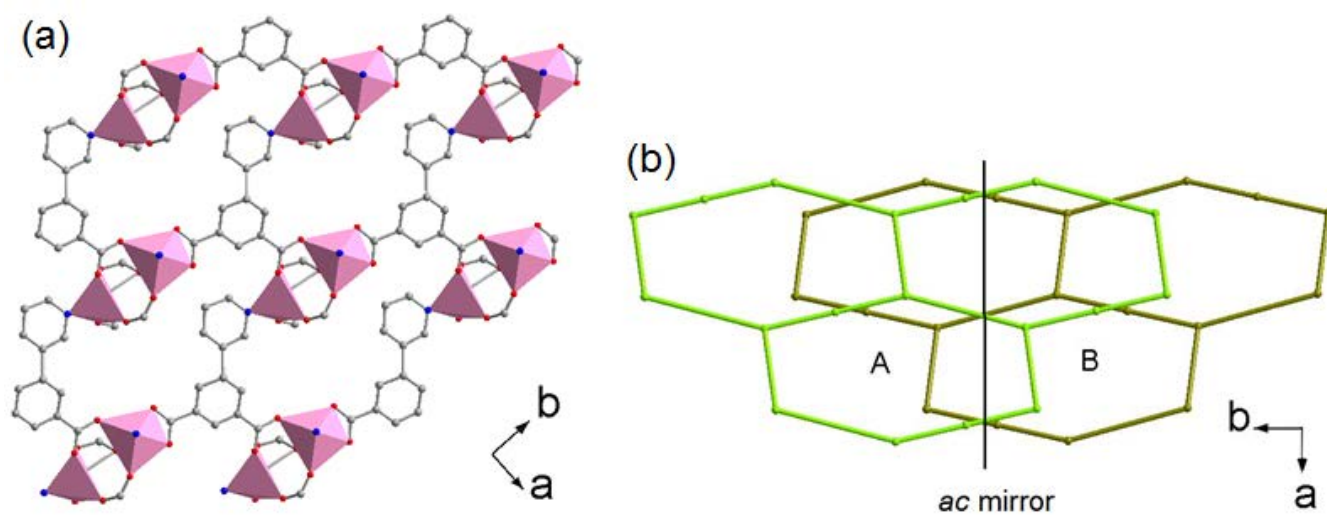
Figure S1. The asymmetric unit of NJU-Bai33.

Figure S2. (a) The 2D **hcb** topological layer (A); (b) The *ac* mirror reflection between layer A and B in NJU-Bai33.
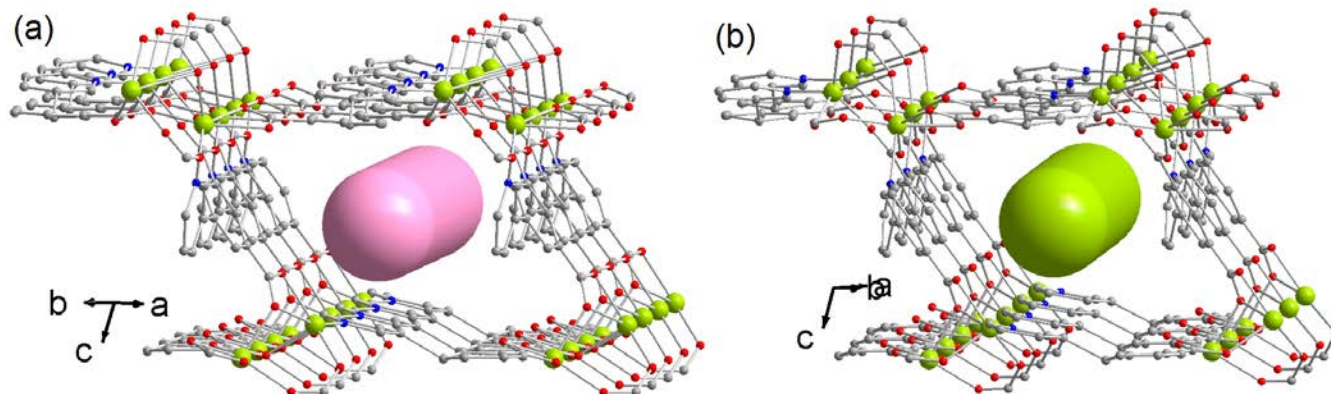
Figure S3. (a) The 1D channel along the direction of (**a**+**b**); (b) The 1D channel along the direction of (**a**-**b**) in NJU-Bai33.
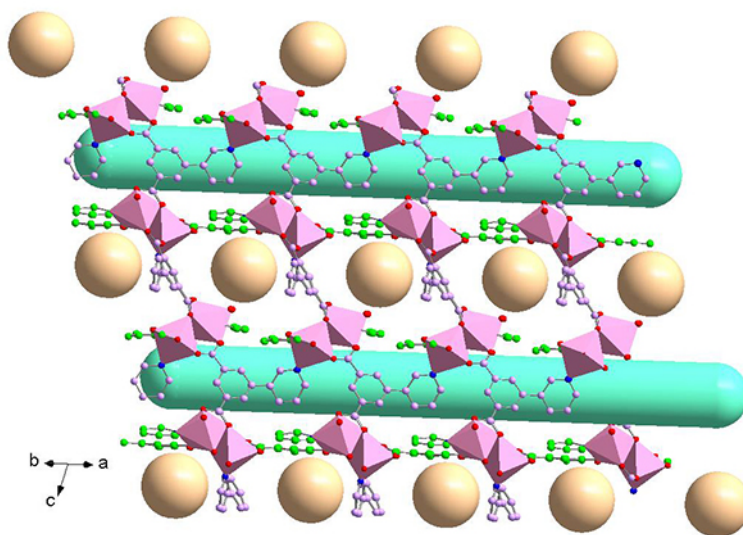

Figure S4. The arrangement of two different kinds of 1D channels in NJU-Bai33. The 1D channel along the direction of (**a**+**b**) (Tan); The 1D channel along the direction of (**a**-**b**) (Turquiose).
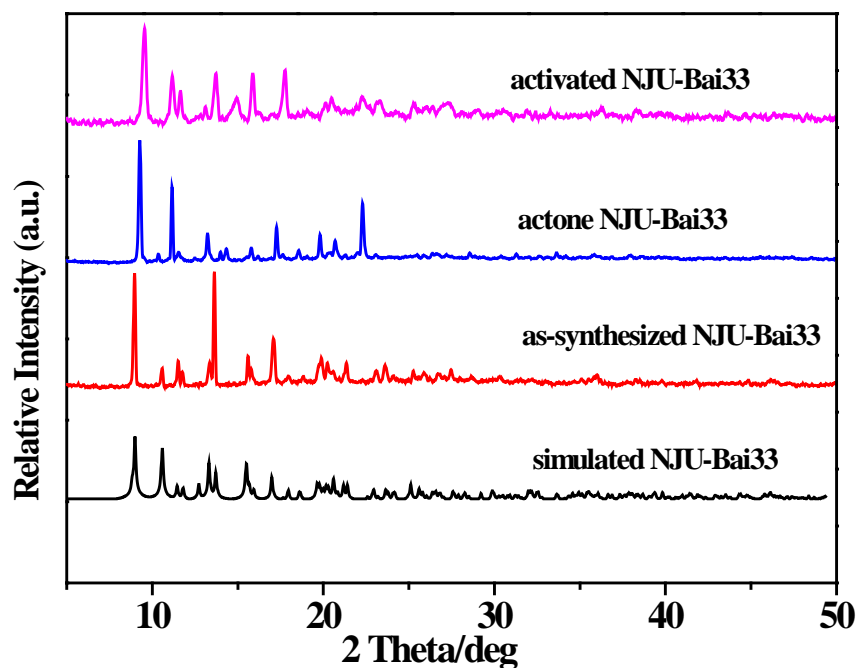
III. PXRD, TG and IR analysis

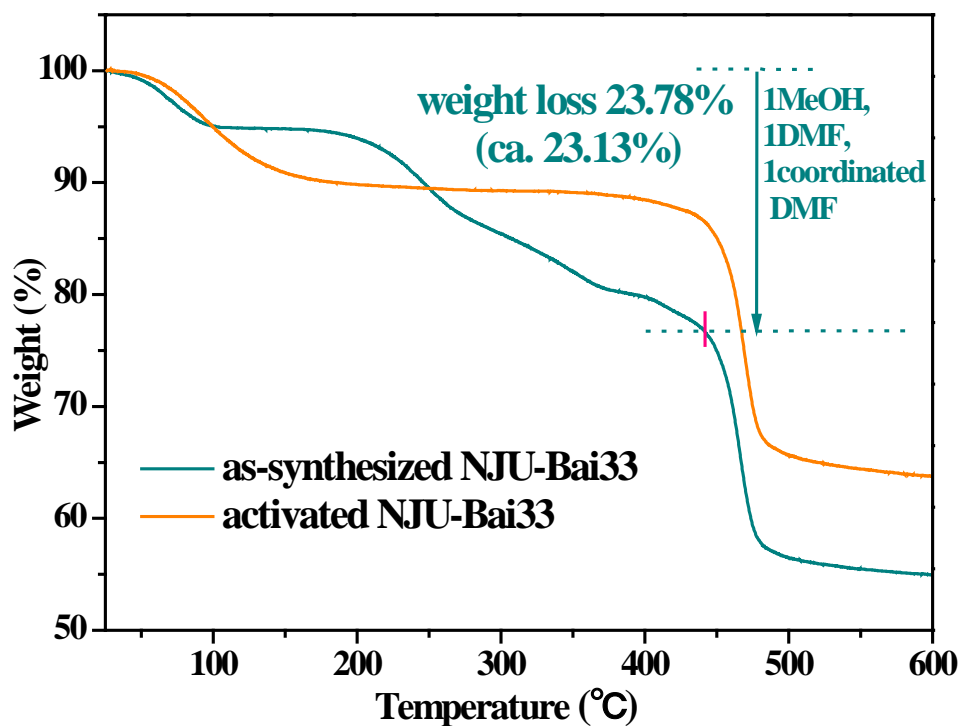**Figure S5.** The PXRD patterns of NJU-Bai33.

Figure S6. TGA curves of as-synthesized (dark cyan) and activated (orange) NJU-Bai33.
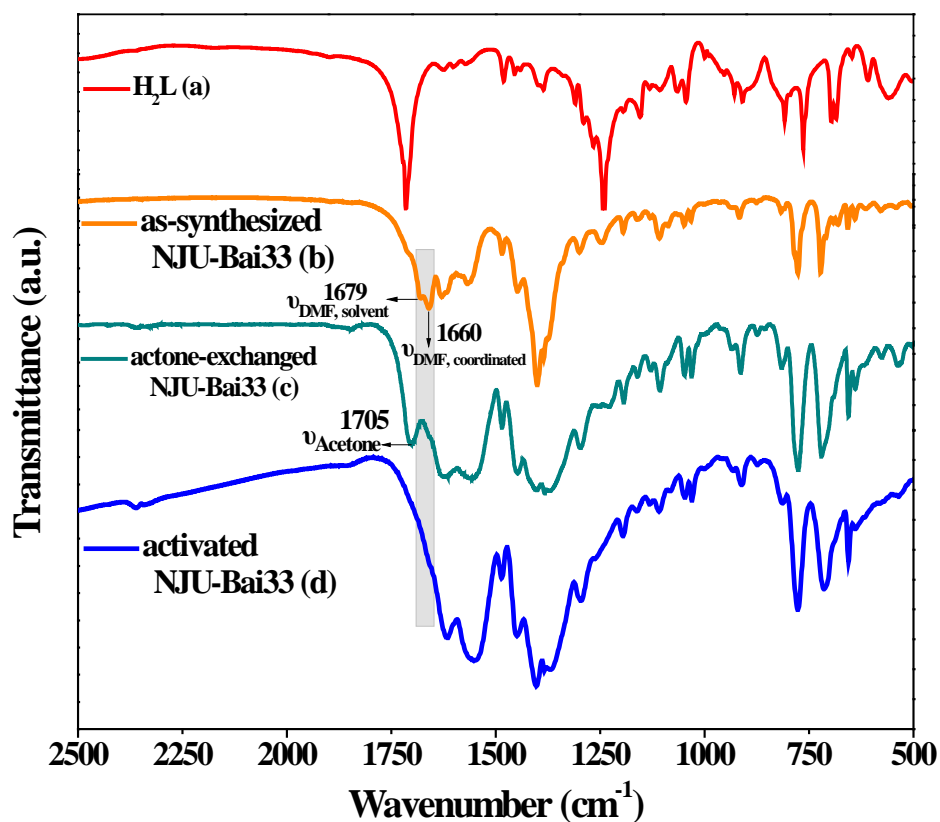
Figure S7. Infrared spectra of (a) ligand, (b) as-synthesized, (c) acetone-exchanged, and (d) activated NJU-Bai33. In the spectrogram of as-synthesized NJU-Bai33 (b), the IR peaks characteristic of C=O stretching of DMF in the pores and coordinated to the Mn(II) ion are evident at 1679 and 1660 cm^{-1}, respectively. The complete removal of DMF molecules in the pores and coordinated to the Mn(II) ion was verified by the disappearance of the vibrations at 1679 and 1660 cm^{-1} in the spectrogram of activated NJU-Bai33 (d).[4]

IV. Low pressure gas sorption measurements

Low-pressure adsorption isotherms of N_2 (99.999%) and CO_2 (99.999%) gases were performed on Quanta chrome Autosorb IQ-2 surface area and pore size analyzer. Before analysis, about 50 mg samples were activated by using the "outgas" function of the surface area analyzer. For all isotherms, ultra-high purity He gas (UHP grade 5.0, 99.999% purity) was used for the estimation of the free space (warm and cold), assuming that it is not adsorbed at any of the studied temperatures. The specific surface areas were determined using the Brunauer-Emmett-Teller (BET) and the Langmuir equation from the N_2 sorption data at 77 K. When applying the BET theory, we made sure that our analysis satisfied the two consistency criteria as detailed by Walton and co-workers.[5] For the Langmuir surface area, data from the whole adsorption data were used.
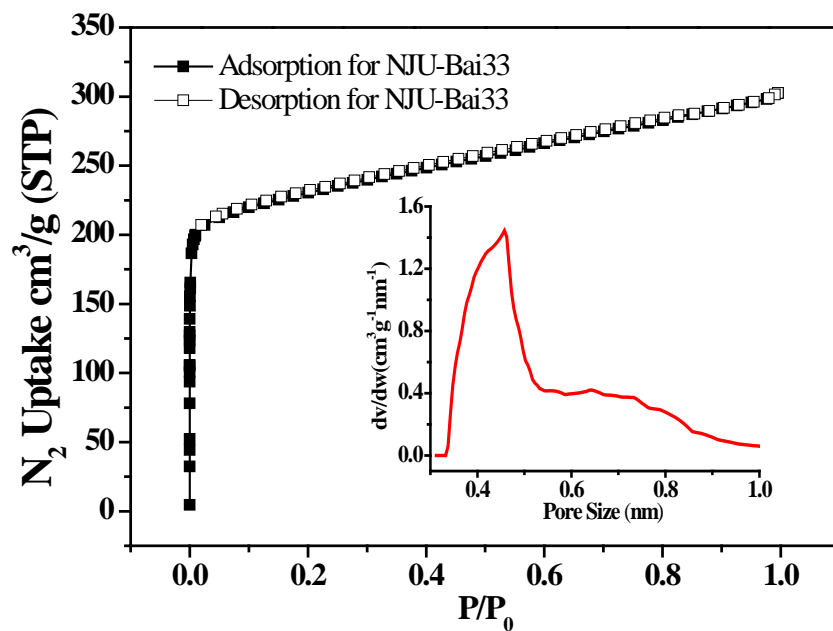
Figure S8. N_2 adsorption isotherms of NJU-Bai33 at 77 K (filled symbols, adsorption; open symbols, desorption); Inset: Horvath-Kawazoe pore size distribution plot of NJU-Bai33.
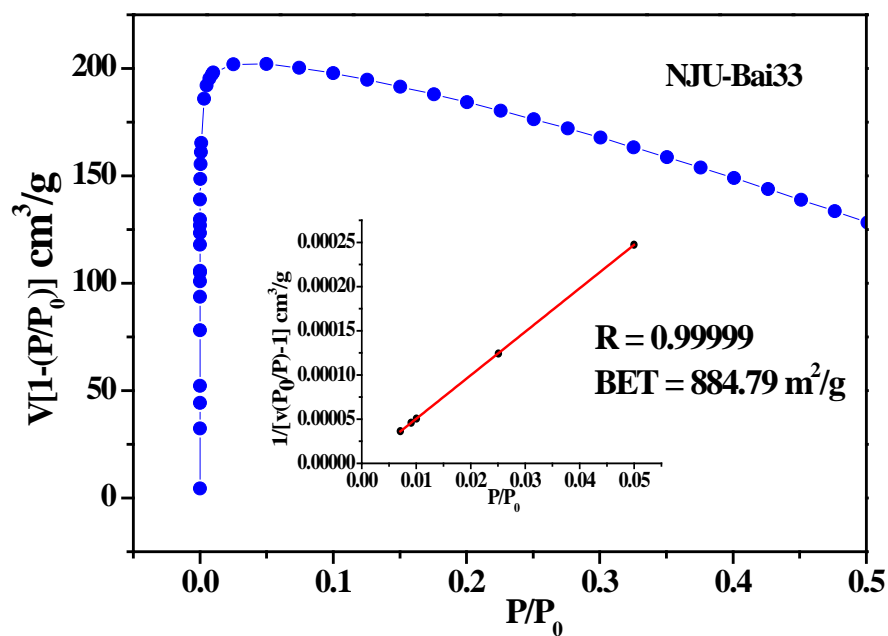

Figure S9. The V[1-(P/P$_0$)] vs. P/P$_0$ for NJU-Bai33, only the range below P/P$_0$ = 0.05 satisfies the first consistency criterion for applying the BET theory. Inset: Plot of the linear region for the BET equation.

Figure S10. CO_2, N_2 and CH_4 adsorption isotherms for NJU-Bai33 at 273 K; Filled and open symbols represent adsorption and desorption, respectively.

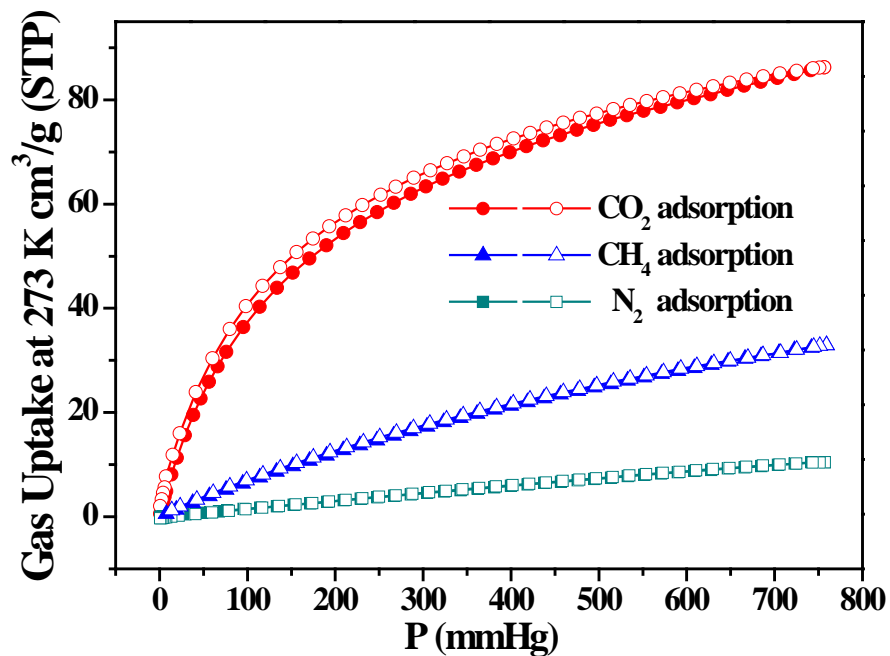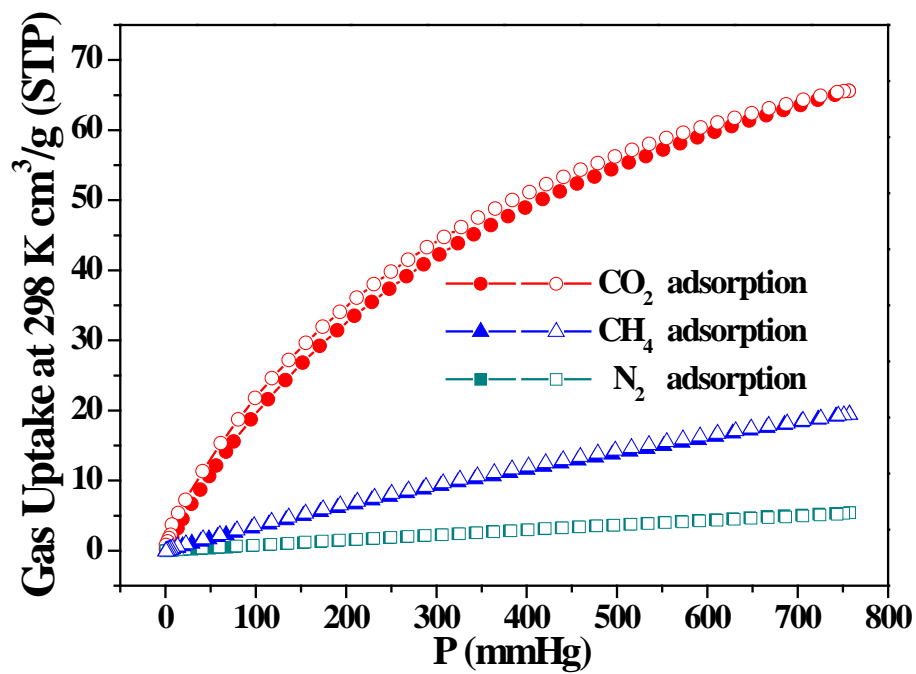***Figure S11.*** CO_2, N_2 and CH_4 adsorption isotherms for NJU-Bai33 at 298 K. Filled and open symbols represent adsorption and desorption, respectively.

V.   Estimation of the isosteric heats of gas adsorption

A virial-type[6] expression comprising the temperature-independent parameters a_i and b_j was employed to calculate the enthalpies of adsorption for CO_2 (at 273 and 298 K) on NJU-Bai33. In each case, the data were fitted using the equation:

$$\ln P = \ln N + 1/T \sum_{i=0}^{m} a_i N^i + \sum_{j=0}^{n} b_j N^j \qquad (1)$$

Here, P is the pressure expressed in Torr, N is the amount adsorbed in mmol/g, T is the temperature in K, a_i and b_j are virial coefficients, and m, n represent the number of coefficients required to adequately describe the isotherms (m and n were gradually increased until the contribution of extra added a and b coefficients was deemed to be statistically insignificant towards the overall fit, and the average value of the squared deviations from the experimental values was minimized). The values of the virial coefficients a_0 through a_m were then used to calculate the isosteric heat of adsorption using the following expression.

$$Q_{st} = -R \sum_{i=0}^{m} a_i N^i \qquad (2)$$

Q_{st} is the coverage-dependent isosteric heat of adsorption and R is the universal gas constant. The heat of CO_2 sorption for NJU-Bai33 in the manuscript are determined by using the sorption data measured in the pressure range from 0-1 bar (273 and 298 K), which is fitted by the virial-equation very well ($R^2 > 0.9999$).
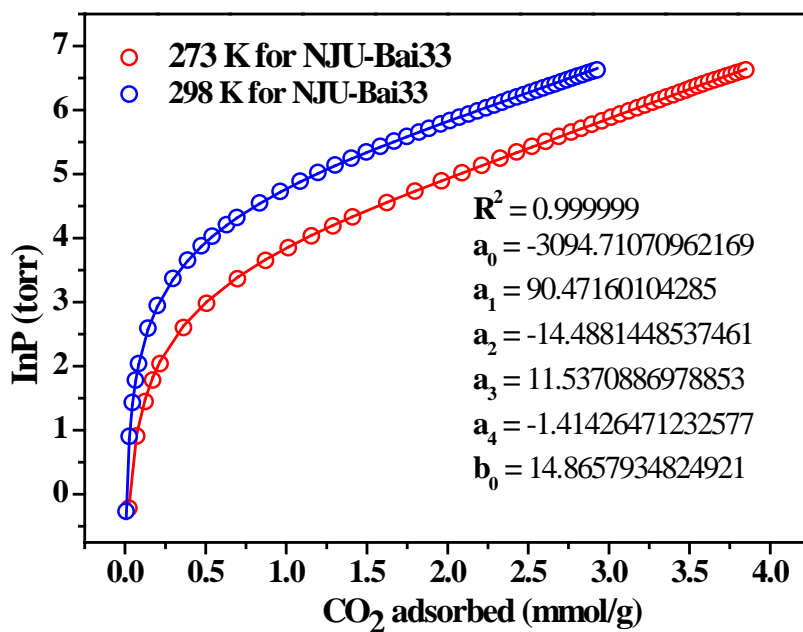
Figure S12. The details of virial equation (solid lines) fitting to the experimental CO_2 adsorption data (symbols) for NJU-Bai33.
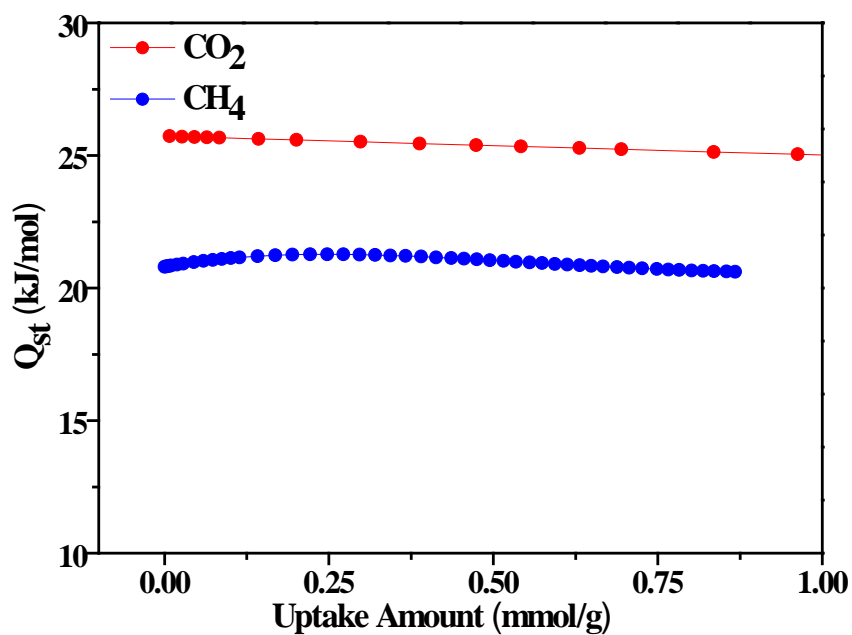

Figure S13. The isosteric CO_2 and CH_4 adsorption enthalpy of NJU-Bai33.

VI. Prediction of the Gases Adsorption Selectivity by IAST

IAST (ideal adsorption solution theory)[7-8] was used to predict binary mixture adsorption from the experimental pure-gas isotherms. In order to perform the integrations required by IAST, the single-component isotherms should be fitted by a proper model. In practice, several methods to do this are available. We found for this set of data that the dual-site Langmuir-Freundlich equation was successful in fitting the data. As can be seen in Figure S14-15 and Table S2-3, the model fits the isotherms very well ($R^2 > 0.9999$).

$$q = \frac{q_{m,1} b_1 p^{1/n_1}}{1 + b_1 p^{1/n_1}} + \frac{q_{m,2} b_2 p^{1/n_2}}{1 + b_2 p^{1/n_2}} \quad (3)$$

Here, P is the pressure of the bulk gas at equilibrium with the adsorbed phase (kPa), q is the adsorbed amount per mass of adsorbent (mmol/g), $q_{m,1}$ and $q_{m,2}$ are the saturation capacities of sites 1 and 2 (mmol/g), b_1 and b_2 are the affinity coefficients of sites 1 and 2 (1/kPa), and n_1 and n_2 represent the deviations from an ideal homogeneous surface. The fitted parameters were then used to predict multi-component adsorption with IAST.

The selectivity $S_{A/B}$ in a binary mixture of components A and B is defined as $(x_A/y_A)/(x_B/y_B)$, where x_i and y_i are the mole fractions of component i ($i = A$, B) in the adsorbed and bulk phases, respectively.

Figure S14. Low pressure gases adsorption isotherms and the dual-site Langmuir-Freundlich (DSLF) fit lines of CO_2, N_2 and CH_4 in NJU-Bai33 at 273 K.

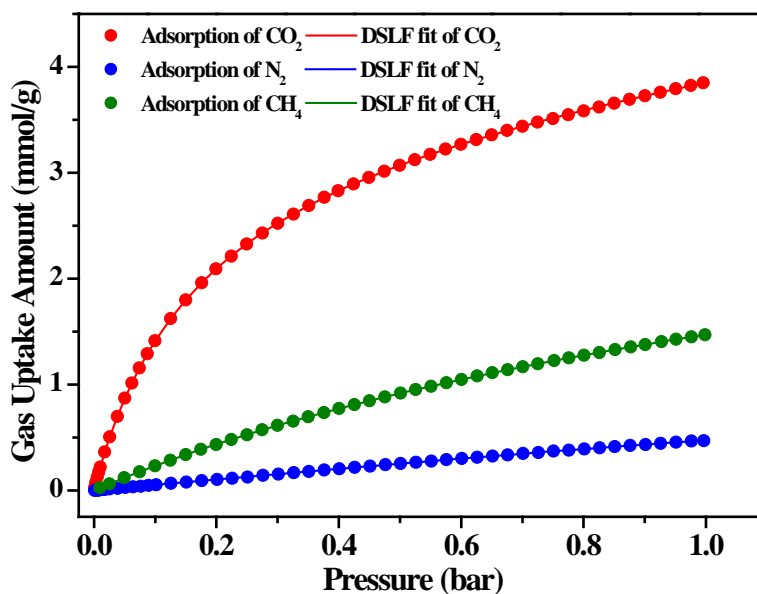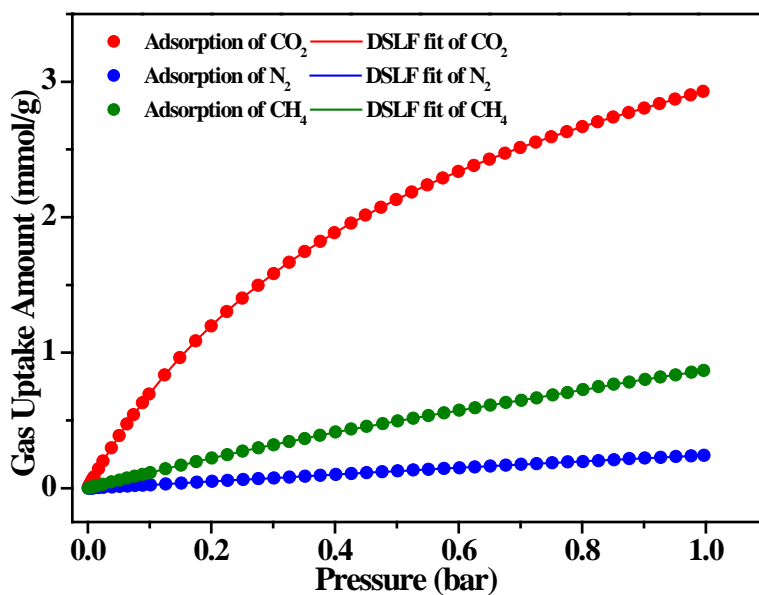***Figure S15.*** Low pressure gases adsorption isotherms and the dual-site Langmuir-Freundlich (DSLF) fit lines of CO_2, N_2 and CH_4 in NJU-Bai33 at 298 K.

Table S2. Dual-site Langmuir-Freundlich parameters for pure CO_2, N_2 and CH_4 isotherms in NJU-Bai33 at 273 K

	NJU-Bai33		
	CO_2	N_2	CH_4
R^2	0.999998542591442	0.999963374838219	0.999997418524626
$q_{m,1}$	1069.26207184977	1.34473380402663	3.85750015022135
$q_{m,2}$	3.59421567281164	0.0409173482509414	0.107259919995291
b_1	9.51952459791818E-06	0.0010816697313452	0.00568537261479121
b_2	0.0598362732119009	0.060263063945008	0.0231598139406771
n_1	0.946943362384502	1.3180294352075	0.994089262512756
n_2	0.980792871024848	1.23556890181235	1.10300935038398

Table S3. Dual-site Langmuir-Freundlich parameters for pure CO_2, N_2 and CH_4 isotherms in NJU-Bai33 at 298 K

	NJU-Bai33		
	CO_2	N_2	CH_4
R^2	0.999998853113238	0.999942641490979	0.999987746355771
$q_{m,1}$	0.155771363266291	1.11167517747295	2.33003443907387
$q_{m,2}$	4.5279961228076	0.00360842720264319	0.0501652702658301
b_1	2.3070355174879E-12	0.00134635187337028	0.00468470100245667
b_2	0.0185652651803463	0.0216060123233633	1.422363238614E-20
n_1	5.60553488354729	1.15048113558132	1.03230021972168
n_2	0.985629518812073	2.26389895383761	10.2191259203714

Figure S16. The fitting initial slopes for CO_2 and N_2 isotherms for NJU-Bai33 collected at 273 K (a) and 298 K (b). CO_2 (red triangle) and N_2 (blue square).
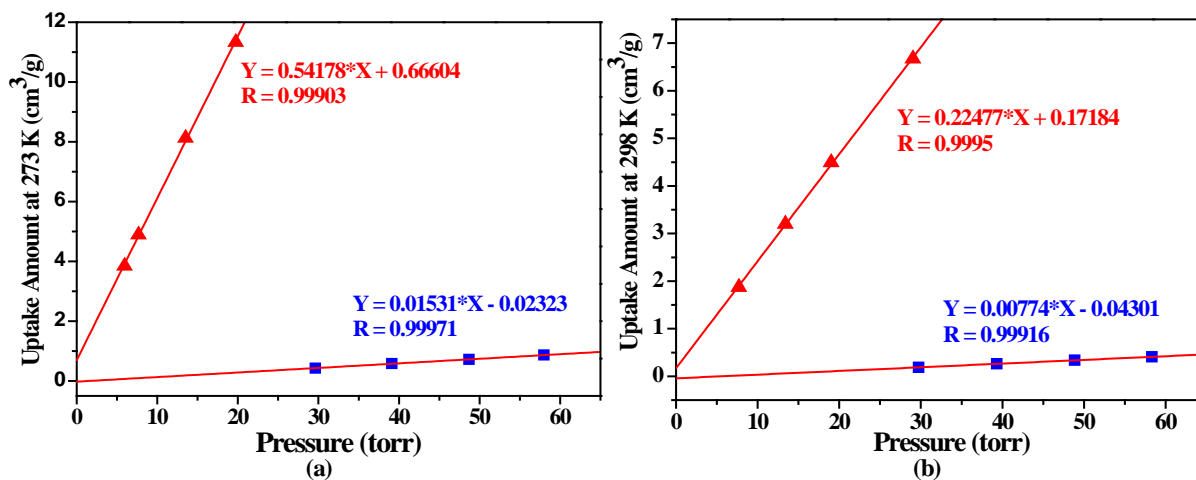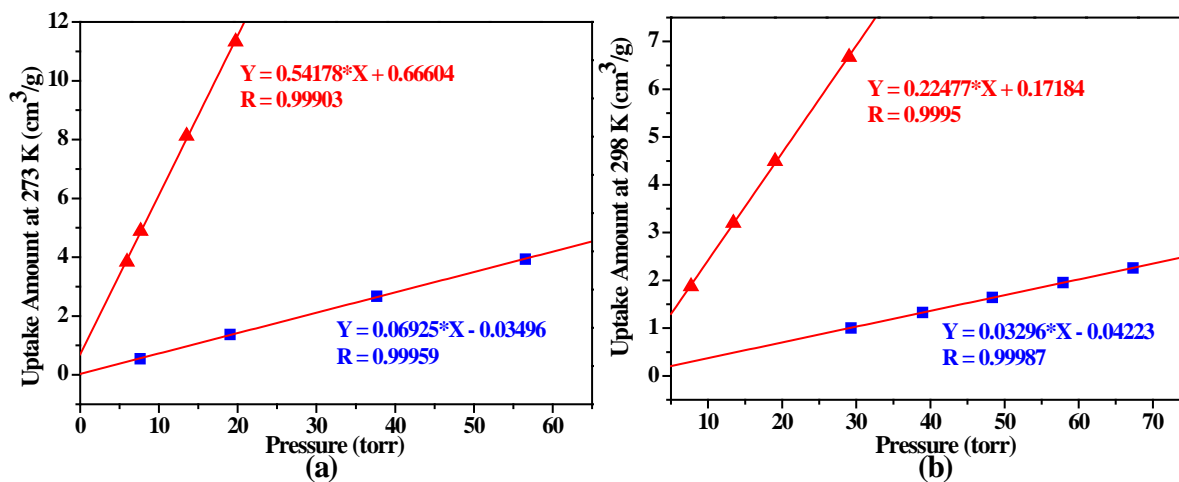

Figure S17. The fitting initial slopes for CO_2 and CH_4 isotherms for NJU-Bai33 collected at 273 K (a) and 298 K (b). CO_2 (red triangle) and CH_4 (blue square).

Table S4. Comparison of selective adsorption for CO_2 of NJU-Bai33 with some typical (3,6)-connected MOFs based upon paddlewheel unit and bifunctional organic ligand with two carboxyl groups and one N donor

MOFs	$Q_{st, CO2}$ (kJ/mol)	Uptake $_{CO2, 273 K}$ (wt%)		Uptake $_{CO2, 298 K}$ (wt%)		$S_{273 K}$[a]		$S_{298 K}$[a]	
		0.15 bar	1 bar	0.15 bar	1 bar	CO_2/N_2	CO_2/CH_4	CO_2/N_2	CO_2/CH_4
NJU-Bai7[9]	40.5	11.8	13.9	8.0	12.8	97.1[b]	14.1[b]	62.8[b]	9.4[b]
[CuL][10]	-	14.7	29.7	7.4	21.8	-	5.3[c]	-	6.8[c]
NJFU-2[11]	38.2	10.6	13.1	6.14	11.6	449.6	96.8	195.1	26.1
NJU-Bai8[9]	37.7	10	12.5	5.4	11.2	111.3[b]	40.8[b]	58.3[b]	15.9[b]
NJU-Bai32[12]	33.5			4.7				48.2	
NJU-Bai33	**25.7**	**7.9**	**16.9**	**4.2**	**12.9**	**58.7**	**9.7**	**40.3**	**8.9**
						36.5[b]	7.8[b]	30.2[b]	6.8[b]
SYSU[9]	28.2	8.0	19.8	3.6	13.4	25.5[b]	4.7[b]	19.0[b]	3.9[b]

a) IAST predicted selectivity for CO_2/N_2 (0.15:0.85) and CO_2/CH_4 (1:1) mixture; *b*) Selectivity calculated from the ratio of initial slopes based upon the isotherms; *c*) IAST predicted selectivity for unspecified CO_2/CH_4 mixture; *d*) H_2L = 5-(1H-Tetrazol-1-yl)isophthalic acid; H_2L_2 = 5-(4-pyridinylmethoxy)isophthalic acid.

Reference

[1] Z.Y. Lu, L.T. Du, K. Z. Tang, J. F. Bai, *Cryst. Growth Des*. **2013**, *13*, 2252.

[2] L. D. Kong, R. Y Zou, W. Z. Bi, R.Q Zhong, W. J Mu, J. Liu, R. P. S. Hana , R. Q Zou, *J. Mater. Chem. A*, **2014**, *2*, 17771.

[3] a) E. Jeong, W. R. Lee, D. W. Ryu, Y. Kim, W. J. Phang, E. K. Kohb, C. S. Hong, *Chem. Commun.*, **2013**, *49*, 2329. b) S. Jeong, J. Choi, M. Park, M. Oh, D. Moon, M. S. Lah, *CrystEngComm*, **2010**, *12*, 2179; c) X. F. Liu, M. Park, S. Hong, M. Oh, J. W. Yoon, J. S. Chang, M. S. Lah, *Inorg. Chem.* **2009**, *48*, 11507. d) D. Danuta; B. J. Lucjan; J. Julia; D. Marek, Crystl. Growth. Des. 2005, *5*, 5.

[4] a) G. M. Sheldrick, *Acta Crystallogr. Sect. A* **2008**, *64*, 112; b) A. L. Spek, *J. Appl. Crystallogr.*, **2003**, *36*, 7.

[5] a) K. S. Walton, K. S. Snurr, *J. Am. Chem. Soc.* **2007**, *129*, 8552; b) J. Rouquerol, P. Llewellyn, F. Rouquerol, *Stud. Surf. Sci. Catal.* **2007**, *160*,49.

[6] J. L. C. Rowsell, O. M. Yaghi, *J. Am. Chem. Soc.* **2006**, *128*, 1304.

[7] A. L. Myers, J. M. Prausnitz, *AIChE J.* **1965**, *11*, 121.

[8] a) Y. S. Bae, K. L. Mulfort, H. Frost, P. Ryan, S. Punnathanam, L. J. Broadbelt, J. T. Hupp, R. Q. Snurr, *Langmuir* **2008**, *24*, 8592; b) B. Mu, F. Li, K. S. Walton, *Chem. Commun.* **2009**, 2493.

[9] L. Du, Z. Lu, K. Zheng, J. Wang, X. Zheng, Y. Pan, X. You and J. Bai, *J. Am. Chem. Soc.*, **2013**, *135*, 562.

[10] S. M. Zhang, Z. Chang, T. L. Hu and X. H. Bu, *Inorg. Chem.*, **2010**, *49*, 11581.

[11] L. Du, Z. Lu, M. Ma, F. Su and L. Xu, *RSC Adv.*, **2015**, *5*, 29505.

[12] Q. Wang, J. Jiang, M. Zhang, and J.Bai, Cryst. Growth Des. 2017, *17*, 16.